layer thickness and the large standard deviation in this parameter are interesting. We speculate that they may be related to the random spread of dopant atoms throughout the doped AlGaAs layer. The discrepancy between measured and estimated drain resistance needs further investigation.

Table 1 SUMMARY OF INVERSE MODELLING PROCEDURE RESULTS

Parameter name	'Inverse modelling' Mean	'Inverse modelling' Standard deviation	Measured value	Unit
		%		
Aluminium fraction	24·9	0·2	25·0	%
Dopant density	1·28	2·3	1·30	$\times 10^{24}\,m^{-3}$
Doped layer thickness	51·1	0·6	51·0	nm
Spacer layer thickness	0·33	48	0·0	nm
Physical gate length	0·24	16	0·25	μm
Source resistance	0·9	20	0·8 average	mΩ m
Drain resistance	1·2	11	0·7 average	mΩ m
Built-in voltage	0·83	2·7	0·80	V
2DEG saturated electron velocity	206	3·9	200*	km/s

* See text for discussion

The saturated electron velocity in the 2DEG was allowed to become a free variable in this inverse modelling procedure to test the self consistency of the work. The mean value of 206 km/s is in good agreement with recent literature[12,13] which suggest a value, due to velocity overshoot and other effects, nearly the commonly accepted peak electron velocity of around 200 km/s.

Conclusion: We have presented a procedure for the inverse modelling of conventional GaAs/AlGaAs HEMTs which for the first time enables the device's structure to be determined from DC I/V characteristic curves. This procedure should be adaptable to other transistor types.

Acknowledgments: The authors thank R. Merrett and P. Mellor from British Telecom Research Laboratories, F. Green, J. Archer, G. Griffiths, W. King and T. Fiossa from the CSIRO Division of Radiophysics, M. Parrilla and A. Parker from Macquarie University and A. Maher and C. Thomas from Sydney University. We thank the CSIRO Division of Radiophysics for their HEMT data and structure measurements, and the CSIRO Institute of Information Science and Engineering for financial support. S. Mahon is a PhD student at Sydney University and thanks OTC Limited for their financial support.

S. J. MAHON
D. J. SKELLERN
Macquarie University
NSW 2109, Australia

2nd November 1990

References

1 LADBROOKE, P., BRIDGE, J., and HILL, A.: 'CAD for GaAs MMIC manufactureability'. Proceeding of the IEEE GaAs IC Symposium, New Orleans, 1990, pp. 335–338
2 LADBROOKE, P.: 'MMIC design, GaAs FETs and HEMTs' (Artech House, London, 1989)
3 HUGHES, W. A., and SNOWDEN, C. M.: 'Nonlinear charge control in AlGaAs/GaAs modulation-doped FET's', *IEEE Trans.*, 1987, **ED-34**, pp. 1617–1625
4 MAHON, S. J., and SKELLERN, D. J.: 'A polynomially based SPICE model for high electron mobility transistors (HEMTs)'. Proceedings of the 1989 International Conference on VLSI and CAD, Seoul, 1989, pp. 125–129
5 PONSE, F., MASSELINK, W. T., and MORKOC, H.: 'Quasi-Fermi level bending in MODFETs and its effect of FET characteristics', *IEEE Trans.*, 1985, **ED-32**, pp. 1017–1023
6 BEDNARCZYK, D., and BEDNARCZYK, J.: 'The approximation of the Fermi–Dirac integral F1/2(n)', *Phys. Lett.*, 1978, **64A**, pp. 409–410
7 DELAGEBEAUDEUF, D., and LINH, N. T.: 'Metal-(n)AlGaAs–GaAs two dimensional electron gas FET', *IEEE Trans.*, 1982, **ED-29**, pp. 955–960
8 PUCEL, R. A., HAUS, H. A., and MORKOC, H.: 'Signal and noise properties of gallium arsenide microwave field-effect transistors', *Adv. in Electronics and Electron Physics*, 1975, **38**, pp. 195–265
9 ROHDIN, H., and ROBLIN, P.: 'A MODFET dc model with improved pinchoff and saturation characteristics', *IEEE Trans.*, 1985, **ED-33**, pp. 664–672
10 BANERJEE, P., BHATTACHARY, P. K., LUDOWISE, M. J., and DIETZE, W. T.: 'High-field transport in organometallic VPE $Al_xGa_{1-x}As$ transfered electron devices', *IEEE Elect. Dev. Lett.*, 1983, **EDL-4**, pp. 283–285
11 WASSERSTROM, E., and MCKENNA, J.: 'The potential due to a charged metallic strip on a semiconductor surface', *Bell Syst. Tech. J.*, 1970, **49**, pp. 853–877
12 FULKERSON, D.: 'Panel session II'. IEEE GaAs IC Symposium, New Orleans, 1990
13 ABE, M., and MIMURA, T.: 'Ultrahigh-speed HEMT LSI technology'. Proceedings of the IEEE GaAs IC Symposium, New Orleans, 1990, pp. 127–130

FAST COMPUTATION OF TWO-DIMENSIONAL DISCRETE COSINE TRANSFORMS USING FAST DISCRETE RADON TRANSFORM

Indexing terms: Algorithms, Transforms

A new fast algorithm is presented for computing the two-dimensional discrete cosine transform (2D DCT) using the fast discrete Radon transform. The algorithm has the lowest number of multiplications compared with other algorithms. Furthermore, the algorithm is well suited for parallel implementation.

Introduction: Since its introduction in 1974, the discrete cosine transform[1] has found wide applications in image processing and data compression, due to its ability to closely approximate the optimal Karhunen–Loeve transform (KLT) and its suitability for implementation by a fast algorithm. Recently, it has been adopted by the CCITT as a part of the video coding standard.

In image coding, the usual way of computing the 2D DCT has been the row column approach, where a 2D DCT of an $N \times N$ block is decomposed into N DCTs of N rows and N DCTs of N columns. A recent study[5] has shown that direct 2D techniques are more efficient than row–column approaches.

We propose a 2D direct computation of the 2D DCT. The approach is based on the geometric relationships between points on a 2D grid, which was exploited by Gertner[3] in his paper on computing the 2D DFT. The 2D DCT is first formulated as a two-dimensional odd DFT (2D ODFT). The newly formed 2D ODFT can be calculated from 3/2 N 1D DFTs and 3/2 N complex multiplications.

Computing of 2D DFT: We briefly describe the discrete Radon transform (DRT) approach to computing a 2D DFT proposed by Gertner,[3] to understand the computation of the 2D DCT. A 2D DFT is defined as

$$X(k,l) = \sum_{i=0}^{N-1}\sum_{j=0}^{N-1} x(i,j)W_N^{ik+jl} \quad k,l = 0,\ldots,N-1 \quad (1)$$

where $W_N = e^{-j2\pi/N}$.

Gertner[3] has shown that an $N \times N$ point 2D DFT can be computed by taking a number of N-point 1D DFTs, where this number is equal to the number of linear congruences of the $N \times N$ grid. The 2D DFT can now be calculated using the

following equations:

$$X(\langle N - ml\rangle_N, l) = \sum_{d=0}^{N-1} R_1(m, d)W_N^{ld} \quad m = 0, 1, \ldots, N-1 \quad (2)$$

$$X(k, \langle N - 2sk\rangle_N) = \sum_{d=0}^{N-1} R_2(s, d)W_N^{kd} \quad s = 0, 1, \ldots, N/2 - 1 \quad (3)$$

where $\langle\rangle_N$ denotes the residue modulo N, R_1 and R_2 are the DRTs on the input array $x(i, j)$, which are defined as

$$R_1(m, d) = \sum_{i=0}^{N-1} x(i, \langle d + mi\rangle_N) \qquad d, m = 0, \ldots, N-1 \quad (4)$$

$$R_2(s, d) = \sum_{i=0}^{N-1} x(\langle d + 2si\rangle_N, i) \qquad d = 0, \ldots, N-1 \quad s = 0, \ldots, N/2 - 1 \quad (5)$$

2D DCT using FDRT: We describe here the algorithm for computing 2D DCT using the FDRT. A 1D DCT is defined as follows:

$$X(k) = \sum_{i=0}^{N-1} x(i) \cos \frac{2\pi(2i + 1)k}{4N} \qquad k = 0, 1, \ldots, N-1 \quad (6)$$

By using a classical mapping[2] the DCT can be written as follows:

$$X(k) = \sum_{i=0}^{N-1} y(i) \cos \frac{2\pi(4i + 1)k}{4N} \quad (7)$$

where $y(i) = x(2i)$ and $y(N - i - 1) = x(2i + 1)$, $0 \le i < N/2$. From trigonometrical identities, the expression for $X(N - k)$ is similar to the above equation except that the cosine function is replaced by a sine function. Hence we can define a transform $U(k)$ as follows:

$$U(k) = X(k) + jX(N - k) = \sum_{i=0}^{N-1} y(i)W_{4N}^{(4i+1)k} \quad (8)$$

Note that we only need to evaluate $U(k)$ for a set of k such that the set $\{k, N - k\} = \{0, \ldots, N - 1\}$.

For the 2D case, the 2D DCT is defined as

$$X(k, l) = \sum_{i=0}^{N-1} \sum_{j=0}^{N-1} y(i, j) \cos \frac{2\pi(2i + 1)k}{4N} \cos \frac{2\pi(2j + 1)l}{4N} \quad (9)$$

By analogy with the 1D case, it is easy to recognise that the 2D DCT coefficients can be obtained from $U(k, l)$ by the following set of equations:

$$\begin{aligned} X(k, l) &= \mathrm{Re}\,[U(k, l) + jU(N - k, l)] \\ X(k, N - l) &= -\mathrm{Im}\,[U(k, l) + jU(N - K, l)] \\ X(N - k, l) &= -\mathrm{Im}\,[U(k, l) - jU(N - k, l)] \\ X(N - k, N - l) &= -\mathrm{Re}\,[U(k, l) - jU(N - k, l)] \end{aligned} \quad (10)$$

where $U(k, l) = \sum_{i=0}^{N-1} \sum_{j=0}^{N-1} y(i, j)W_{4N}^{(4i+1)k+(4j+1)l}$. Note that eqn. 10 requires $U(k, l)$ to be computed for all k, and only a subset of l such that $\{1, N - 1\}$ cover all possible values of l.

We can describe $U(k, l)$ as follows:

$$U(k, l) = W_{4N}^{k+j} \sum_{i=0}^{N-1} \sum_{j=0}^{N-1} y(i, j)W_N^{ik+jl} \quad (12)$$

and observe that the summation in the above equation is exactly that for the 2D DFT. Hence the computation of the 2D DCT can be performed by the discrete Radon transform in Reference 3, giving

$$U(\langle N - ml\rangle_N, l) = W_{4N}^{\langle N-ml\rangle_N + l} \sum_{d=0}^{N-1} R_1(m, d)W_N^{ld} \quad (13)$$

$$U(l, \langle N - 2ml\rangle_N) = W_{4N}^{\langle N-2ml\rangle_N + l} \sum_{d=0}^{N-1} R_2(m, d)W_N^{ld} \quad (14)$$

The computation of a 2D DCT can now be performed by a number of 1D DFTs with one additional complex multiplication. Note that this approach is more efficient than the 2D DFT plus $2N$ complex multiplications, as the number of linear congruences in a $N \times N$ grid is $\le 2N$. In addition, the computation of sets of Radon transforms and their DFTs can be performed independent of one another. So we can have $(3/2N)$ processors running in parallel, with each process computing the 1D DFT and complex multiplication, simultaneously.

Arithmetic complexity: Let $M[]$ and $A[]$ denote the number of multiplications and additions needed to compute [], respectively. The arithmetic complexity for the FDRT-based 2D DFT algorithm for real inputs are[4]

$$\begin{aligned} M[\mathrm{DFT}\,(2^n \times 2^n)] &= n2^{2n-1} - \tfrac{7}{3}2^{2n-1} + \tfrac{8}{3} \\ A[\mathrm{DFT}\,(2^n \times 2^n)] &= 3n2^{2n} - 2^{2n+1} + 18 \end{aligned} \quad (15)$$

Because the number of linear congruences for the $N \times N$ array with $N = 2^n$ is $3\,2^{n-1}$, the number of additional complex multiplications is $3/2N$. Furthermore, a complex multiplication can be implemented by three real multiplications and three real additions. Therefore, the arithmetic complexity for the FDRT-based 2D DCT are

$$\begin{aligned} M[\mathrm{DCT}\,(2^n \times 2^n)] &= n2^{2n-1} - \tfrac{7}{3}2^{2n-1} + \tfrac{8}{3} + 92^{n-1} \\ A[\mathrm{DCT}\,(2^n \times 2^n)] &= 3n2^{2n} - 2^{2n+1} + 18 + 92^{n-1} \end{aligned} \quad (16)$$

The measure of computational complexity of the proposed algorithm is shown in Table 1 together with other algorithms for comparison. In this comparison, one complex multiplication is evaluated by three real multiplications and three real additions. Note that the proposed algorithm requires significantly fewer multiplications and only slightly more additions.

Conclusion: In this letter a novel fast algorithm for computing the 2D DCT is described. The proposed algorithm requires the minimum number of multiplications compared with other related algorithms. Further reduction in computational complexity may be achieved by examining the redundancies that occur in the mapping DCT to DFT. In addition, the algorithm is well suited for parallel implementation.

N. TA
Y. ATTIKIOUZEL
G. CREBBIN

Department of Electrical and Electronic Engineering
The University of Western Australia
Nedlands, Western Australia 6009, Australia

5th November 1990

Table 1 ARITHMETIC COMPLEXITY OF $N \times N$ 2D DCT ALGORITHMS

	Proposed algorithm		Polynomial transform		Row-column FFCT[2]	
N	Multiplication	Addition	Multiplication	Addition	Multiplication	Addition
8	60	512	96	484	192	464
16	288	2650	512	2531	1024	2592
32	1512	13474	2560	12578	5120	13376
64	7800	65842	12288	60578	24576	65664

References

1 AHMED, N., NATARAJAN, T., and RAO, K. R.: 'Discrete cosine transform', *IEEE Trans.*, 1974, **C-23**, pp. 90–93

2 VETTERLI, M., and NUSSBAUMER, H. J.: 'Simple FFT and DCT algorithms with reduced number of operations', *Signal Processing*, 1984, **6**, pp. 267–278

3 GERTNER, I.: 'A new efficient algorithm to compute the two-dimensional discrete Fourier transform', *IEEE Trans.*, 1988, **ASSP-36**, pp. 1036–1050

4 YANG, D.: 'Fast discrete Radon transform and 2-D discrete Fourier transform', *Electron. Lett.*, 1990, **26**, (8), pp. 550–551

5 DUHAMEL, P., and GUILLEMOT, C.: 'Polynomial transform computation of the 2-D DCT'. Proc. IEEE ICCASSP '90, 1990, pp. 1515–1518

6 NARASIMHA, M. J., and PETERSON, A. M.: 'On the computation of the discrete cosine transform', *IEEE Trans.*, 1978, **COM-26**, pp. 934–936

ELECTRON MOBILITY AND DEEP LEVEL TRAP PROFILES OF MBE GaAs ON Si MESFETs

Indexing terms: Electron mobility, Field effect transistors

Low field electron mobility and deep trap profiles have been determined for 0·7 μm gate length GaAs on Si MESFETs. The peak mobility at 300 K is 3600 cm^2/V s, and the dominant trap has been identified as EL2 (E_a 0·83 eV), with a concentration of 2–6 $\times$ 10^{14} cm^{-3}. The comparison of these profiles with those of GaAs/GaAs MESFETs has been used to assess the electrical effects of growth on a silicon substrate.

Introduction: The monolithic integration of gallium arsenide and silicon technologies has attracted considerable attention; reports have included discrete GaAs/Si MESFETs with an RF performance at 8 GHz equal to GaAs/GaAs devices,[1] and a 1 Kbit static RAM using GaAs/Si MESFETs with an access time of 6–14 ns.[2] However the high density of dislocations (10^7–10^8 cm^{-2}) at the GaAs–Si interface can reduce the quality of the GaAs layer,[3] and concern exists that this may cause detrimental effects on device performance and reliability,[2,3] for example by the autodiffusion of silicon.[4] We report for the first time profiles of low field electron mobility and deep level traps in GaAs/Si MESFETs, and compare these with profiles from GaAs/GaAs MESFETs.

Layer growth and device fabrication: GaAs/GaAs and GaAs/Si layers were grown using MBE, on semi-insulating GaAs and 80 Ω cm resistivity silicon substrates. For both device types the growth sequence was: 2 μm undoped GaAs buffer layer, 0·2 μm channel layer n-GaAs : Si 1–2 $\times$ 10^{17} cm^{-3}, 0·05 μm cap layer n^+-GaAs : Si 2 $\times$ 10^{18} cm^{-3}. Depletion mode devices were fabricated with evaporated InGeAu ohmic contacts and TiPtAu gate metallisation. The GaAs/GaAs devices had a transconductance of 175 mS/mm compared with 170 mS/mm for the GaAs/Si MESFETs.

Results: GaAs on GaAs MESFETs: Using current deep level transient spectroscopy[5] (DLTS) two nonexponential current transients were detected, and a typical spectrum is shown in the inset to Fig. 1. The transients had peak amplitudes of 10–20 μA, which correspond to trap concentrations of 2–4 $\times$ 10^{15} cm^{-3}. Fig. 1 shows the variation of transient current amplitude with trap filling pulse for the electron trap shown in the DLTS spectrum. There was no deep trapping close to open channel conditions, with the transient current increasing to a maximum close to the pinch-off voltage (V_p). Hence this trap has a highly nonlinear distribution, with the peak concentration located close to the channel-buffer interface. The hole trap-like transient is similar to that reported by Hickmott *et al.*[6] and identified as being due to deep trapping near to the channel/buffer interface, at low temperatures.

Fig. 1 also shows the electron mobility profile at 300 K which was determined from geometric magneto-transconductance measurements.[7] The rapid decrease in mobility towards pinch-off has been reported before,[7] and attributed to a reduction in ionised impurity screening.[8] However this does not explain the similar rapid decrease in the mobility of MESFET layers reported from Hall effect strip and etch measurements.[9] From the GaAs/GaAs profile in Fig. 1 it can be seen that the rapid decrease in mobility coincides with the onset of deep trapping.

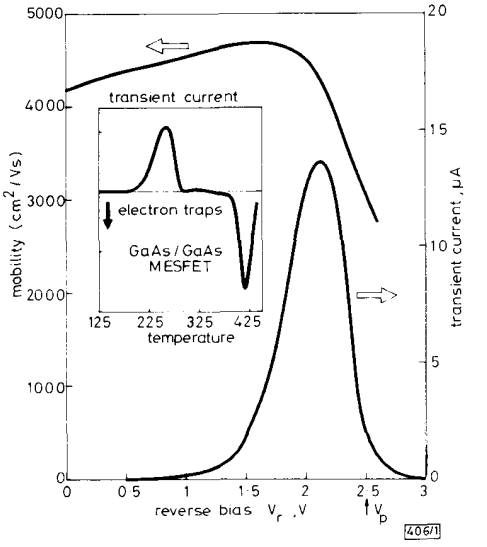

Fig. 1 *Electron mobility and deep trap profiles for GaAs/GaAs MESFET*

Results: GaAs on Si MESFETs: A single electron trap was detected with an activation energy 0·83 eV and a capture cross-section of 3 $\times$ 10^{-13} cm^2, which corresponds to the signature of the GaAs trap EL2.[10,11] The transient current amplitudes were 1–3 μA, equivalent to a concentration of 2–6 $\times$ 10^{14} cm^{-3}. Fig. 2 shows the variation of the transient current with reverse bias for EL2, together with the 300 K low field electron mobility profile for the same device. From the relatively linear dependence of transient current amplitude with trap filling pulse it can be deduced that the EL2 is approximately uniformly distributed in the channel. In con-

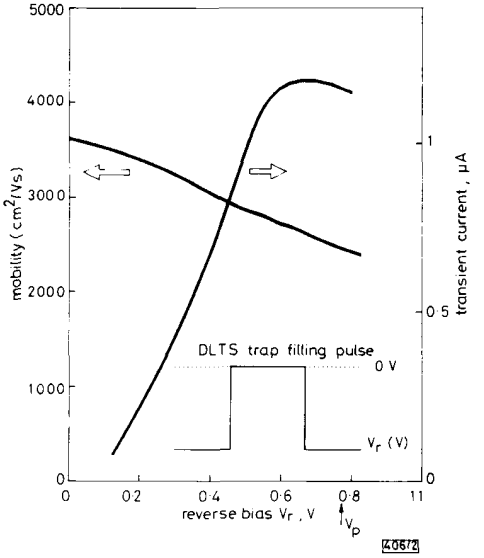

Fig. 2 *Electron mobility and EL2 profiles for GaAs/Si MESFET*